





RESEARCH ARTICLE | AUGUST 11 2023

Characteristics of clustered particle relative velocity in homogeneous and isotropic turbulence

Tuo Li (李拓) ; Xinyang Li (李心阳) ; Huan Lian (连欢)  



Physics of Fluids 35, 085121 (2023)

<https://doi.org/10.1063/5.0157869>



Physics of Fluids

Special Topic: Overview of Fundamental and Applied Research in Fluid Dynamics in UK

[Submit Today](#)



Characteristics of clustered particle relative velocity in homogeneous and isotropic turbulence

Cite as: Phys. Fluids **35**, 085121 (2023); doi: [10.1063/5.0157869](https://doi.org/10.1063/5.0157869)

Submitted: 12 May 2023 · Accepted: 20 July 2023 ·

Published Online: 11 August 2023






View Online



Export Citation



CrossMark

Tuo Li (李拓),^{1,2}  Xinyang Li (李心阳),^{1,2}  and Huan Lian (连欢)^{1,a)} 

AFFILIATIONS

¹State Key Laboratory of High Temperature Gas Dynamics, Institute of Mechanics, Chinese Academy of Sciences, Beijing 100190, China

²School of Engineering Science, University of Chinese Academy of Sciences, Beijing 100049, China

^{a)}Author to whom correspondence should be addressed: hlian@imech.edu.cn

ABSTRACT

Particle collisions are mainly governed by the preferential concentration of inertia particles and the formation of fold caustics. By fold caustics, we mean that relative velocity does not go smoothly to zero when the particle separations decrease due to inertia. Despite the importance of the second-order relative velocity structure function, there has been relatively little experimental research on the formation of caustics due to the high accuracy requirements for the particle relative velocity measurements. In the dissipation range, an obvious departure between the second-order structure function of particles normalized by the square of the Kolmogorov velocity and the Kolmogorov turbulent scaling of r^{-2} was observed for all four experimental conditions. In the inertial range, the second-order structure function normalized by the square of the Kolmogorov velocity was consistent with the scale form of $r^{2/3}$ in all cases. The conditional second-order relative velocity structure function of particles in clusters differs from that of the arithmetically averaged particle statistics in both the dissipation range and the inertial subrange. In the dissipation range, caustics are present for all categories of particles. In the inertial range, the scaling of the second-order velocity structure function is almost identical for all categorized particle types.

Published under an exclusive license by AIP Publishing. <https://doi.org/10.1063/5.0157869>

I. INTRODUCTION

An understanding of turbulent dispersed particle dynamics is fundamental in developing parameterizations and models of natural and industrial applications. Such dynamics occur in aerosols and rain-drop formation in terrestrial clouds, dust grain dynamics in astrophysical environments, such as interstellar media, and turbulent spray combustion in propulsion systems. The collisions of small particles suspended in the turbulent flow have a profound influence on the settling velocity, growth rate, and evaporation. Sundaram and Collins¹ proposed the collision kernel model, which calculates the collision rate of two particles per unit volume of fluid. This model requires the inertial particle pair statistics of the radial distribution function (RDF)² at contact and the mean inward relative velocity along the line of the two particle centers. The collision kernel is corrected by the RDF for non-uniform spatial distributions of particles caused by clustering or preferential concentration (i.e., when inertial particles accumulate in regions of low vorticity and high strain rate³). The collision rate at which the particles encounter each other is controlled by the inward

relative velocity. Thus, particle collisions are mainly governed by the preferential concentration of inertia particles and the formation of fold caustics, whereby very close particles exhibit large relative velocities.⁴ The first effect of preferential concentration suggests that inhomogeneous particle distributions will be created. Previous studies have provided fruitful information on the quantifications and underlying mechanisms. Most research has focused on the quantification of the clustering phenomenon.^{1,3,5-9} In addition, there have been several investigations of the underlying clustering mechanisms.¹⁰⁻²⁶ The second effect is the formation of fold caustics, which enables very close particles to exhibit large relative velocities. The studies of Falkovich *et al.*,²⁷ Falkovich and Pumir,²⁸ and Wilkinson *et al.*²⁹ have drawn attention to the role played by caustics, which are finite-time singularities in the particle velocity field caused by inertial particles not exactly following the fluid flow.³⁰ Consequently, particles from different flow regions, with different histories, may occupy the same position, producing inertial particle velocity fields that do not require a single value at the given point. This occurrence is also known as crossing

trajectories³¹ or the sling effect.^{27,28} These studies have proved that caustics can increase the collision rate significantly. Bec *et al.*⁴ studied the low-order velocity structure function of inertial particles in the dissipation range and proved that the power coefficients are functions of the Stokes number (St) through direct numerical simulations. They found that the spatial dependence of the structure function completely disappeared when $St > 7$, implying the existence of caustics. Bewley *et al.*³² developed a time-resolved three-dimensional particle tracking velocimetry (PTV) method to observe both the sling effect and crossing trajectories between particles. The particle positioning and pairing accuracy were improved based on the two-frame holographic method by de Jong *et al.*,¹⁴ who presented the first measurements of relative velocities among inertial particles in a homogeneous isotropic turbulent flow. Their results indicated excellent agreement between experimental measurements and direct numerical simulations of the RDF, capturing the inertial clustering effect.¹² Dou *et al.*³³ studied the dependence of radial relative velocity on St and the Taylor-scale Reynolds number Re_λ in isotropic turbulence ($246 < Re_\lambda < 357$) based on a four-frame planar PTV system. Yavuz *et al.*³⁴ reported the first ultra-high-resolution sub-Kolmogorov ($r/\eta \approx 0.2$) RDF measurements of particles in isotropic turbulence ($155 < Re_\lambda < 314$) using a three-dimensional PTV technique and explained the sub-Kolmogorov clustering phenomenon based on a Stokes-flow description of two spheres, in which the mutual hydrodynamic interaction and perturbative small-inertia expansion govern the small-scale dynamics.

To date, most experimental efforts have focused on the first-order relative velocity statistics and the RDF or Voronoi quantification of the particle preferential concentration. Despite the importance of the second-order relative velocity structure function, there has been relatively little experimental research on the formation of caustics due to the high accuracy requirements of particle relative velocity measurements. In addition, the coupling effects between preferential clustering and the particle caustics formation have not been examined numerically or experimentally, because most numerical work depends on the point particle assumption and the classic Maxey–Riley–Gatignol (MRG) equation of motion.^{35–37} The derivation of the MRG equation requires Re_p to vanish so that different forces can be linearly superposed and the interparticle effects can be ignored.

As a means of targeting these two issues, and to provide experimental evidence for the formation mechanism of caustics, this paper

reports high-resolution particle velocity measurements from the dissipation range to the inertial subrange and provides a careful evaluation of the second-order relative velocity structure functions. There are indeed caustics in the dissipation range of the second-order velocity structure function of the particles under two Stokes and Reynolds numbers. By categorizing the particles into clusters and voids based on Voronoi tessellation, we show for the first time that the conditional statistics of the second-order relative velocity structures of particles in clusters are low in kinetic energy and are different from the arithmetically averaged particle statistics in both the dissipation range and the inertial subrange. The remainder of this paper is organized as follows. The measurement techniques and the experimental apparatus are introduced in Sec. II, and the results and discussion are detailed in Sec. III. Finally, the conclusions to this study are given in Sec. IV.

II. EXPERIMENTAL SETUP

The experimental facility consists of an open chamber where zero-mean-flow homogeneous and isotropic turbulence (HIT) is produced by eight woofers. The chamber is built within a cubic frame box constructed by 1 m length aluminum profiles such that the open chamber configuration provides good optical access. The eight woofers are mounted on in particular, designed aluminum plates installed at the eight corners of the cubic box, and point toward the center of the box. The vibrations of the speaker membrane during operation induce ambient air motions and uniform arrays of jets are produced by mounting perforated PVC plates with 55 holes of diameter 6 mm arranged in a triangular mesh pattern on top of each woofer. The experimental arrangement of the turbulence box with the eight woofers is illustrated in Fig. 1(a). It should be noted that both the two-dimensional particle image velocimetry (PIV) system and the three-dimensional tomographic PIV are illustrated in Fig. 1(a). In the current paper, only the two-dimensional measurement results are reported. Homogeneity and isotropy are achieved with a volume of approximately $50 \times 50 \times 50 \text{ mm}^3$ at the center of the box.³⁸ The turbulence box is located in a closed room equipped with an air purifier to avoid contaminant interference. Supplemental frames are assembled on top of the box to support particle screw feeders and a spray atomizer. Particles or droplets are fed by gravity toward the center of the box. The intensity of the synthetic jets is directly relevant to the vibration of the speaker membrane, which is controlled by a sine wave voltage signal characterized by its frequency, amplitude, and phase. When

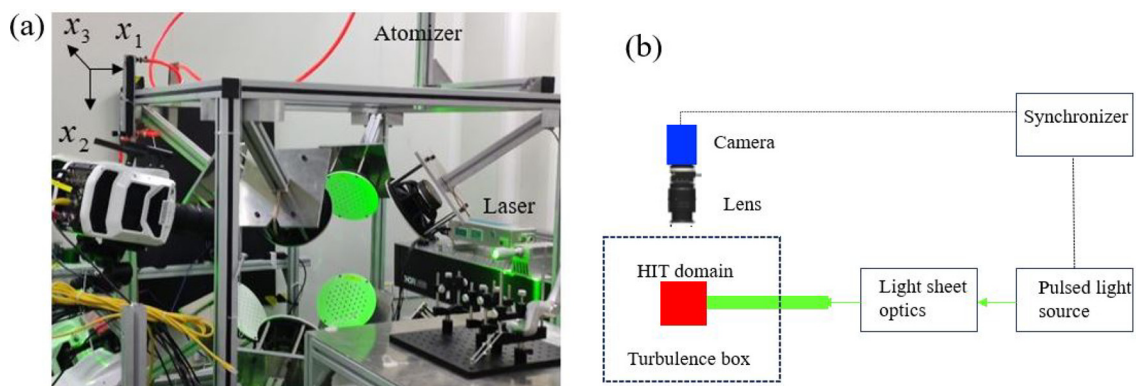


FIG. 1. (a) Setup of the droplet-laden homogeneous and isotropic turbulence experiment. (b) Sketch of the experimental setup.

the frequency of the sine wave increases, the membranes vibrate faster. The vibrations are enhanced when the amplitude of the sine wave increases, and the phase of the sine wave determines the axial movement direction of the speaker membrane. In our case, by controlling the amplitude of the sine wave driving each woofer, the intensity of the synthetic jets can be precisely controlled. The sine waves are generated by a 16-bit National Instruments analogue output card with eight channels (PCI6733), controlled by a program developed in the Labview environment. To provide a sufficient voltage to drive the speakers, the power outputs of these sine waves are amplified by Behringer Europower EP2500 audio stereo amplifiers. A particle image velocimetry (PIV) system is used to measure the two-dimensional fluid velocity. Before obtaining the measurements, the flow field is seeded with tracer particles, which are assumed to follow the flow. In our case, we use a fog generator to produce micrometer-sized particles. The fog generator is located at one end of the room so that the turbulence box can be homogeneously seeded with tracer droplets. The measurement parameters are summarized in Table I. The air flow is seeded with 3- μm organic oil drops as tracer particles produced by a high-temperature particle generator. A dual-head Nd:YAG laser with a wavelength of 532 nm and a maximum energy of 200 mJ pulse⁻¹ generates a laser beam that passes through a carefully designed lens group and forms a laser sheet with a thickness of approximately 1 mm. A double-exposure ultra-high-resolution CCD camera (IMPERX ICL-B6640, 12 bit) with an active sensor size of 6600 \times 4400 pixels² is equipped with a 180-mm lens to capture the particles in the measurement domain with a digital image resolution of 12 μm pixel⁻¹. The sampling frequency is 1 Hz, and 1800 uncorrelated realizations are recorded for each Re_λ (Reynolds number based on transverse Taylor microscale λ_T). A state-of-the-art cross correlation algorithm with window deformation and multi-resolution iterations³⁹ is used for the velocity field calculation. The interrogation window of the final pass is 32 \times 32 pixels² with an overlap ratio of 75%. Therefore, the spatial resolution of the velocity field is 0.42 mm ($\sim 2\eta$, where η is the Kolmogorov length scale) with a vector spacing of 0.1 mm ($\sim 0.5\eta$), which is considered to be appropriate for capturing fine-scale turbulent flows without significant bias.⁴⁰ As illustrated in Fig. 1(a), the horizontal direction x_1 and gravity direction x_2 are defined in the measurement plane, and the corresponding velocity components are u_1 and u_2 , respectively. The *rms* subscript of the velocities denotes the corresponding root-mean-squared fluctuation intensities, and the

TABLE I. Experimental configurations.

Camera	IMPERX-B6640 CCD
Lens	Tamron 180 macro lens
Sampling frequency	1 Hz
Sensor size	6600 \times 4400 pixel
Measurement domain of interest	53 \times 53 mm ²
Digital image resolution	12 μm /pixel
Sampling number	1800
Final interrogation window	32 \times 32 px ²
Overlap ratio	75%
PIV spatial resolution	0.42 mm ($\sim 2\eta$)/vector
PIV vector spacing	0.1 mm ($\sim 0.5\eta$)

subscripts f and p denote fluid and discrete phase variables, respectively. The present experiment considers two Re_λ cases by adjusting the input voltage of the woofers. The basic HIT parameters for the two Re_λ values are summarized in Table II. Zhu *et al.*³⁸ have reported the homogeneity and isotropy conditions of the present turbulent flows and discussed path-history effect at small scales. The basic parameters listed in Table II and their methods of evaluation have been described by Frisch.⁴¹ For a given viscosity coefficient and dissipation rate, the Kolmogorov length scale, velocity scale, and timescale of the minimum vortex structure can be calculated from the following three equations:

$$\eta = (\nu^3/\varepsilon)^{1/4}, \tag{1}$$

$$u_\eta = (\varepsilon\nu)^{1/4}, \tag{2}$$

$$\tau_\eta = (\nu/\varepsilon)^{1/2}. \tag{3}$$

ν is the kinematic viscosity of the carrier phase fluid. The dissipation rate ε is related to the velocity spatial gradient through the following equation (two-dimensional form) in homogenous turbulence:

$$\varepsilon = 4\nu \left[\left\langle \left(\frac{\partial u_1}{\partial x_1} \right)^2 \right\rangle + \left\langle \left(\frac{\partial u_2}{\partial x_2} \right)^2 \right\rangle + \left\langle \frac{\partial u_1}{\partial x_1} \frac{\partial u_2}{\partial x_2} \right\rangle + \frac{3}{4} \left\langle \left(\frac{\partial u_2}{\partial x_1} + \frac{\partial u_1}{\partial x_2} \right)^2 \right\rangle \right]. \tag{4}$$

The ensemble-averaged turbulent kinetic energy q^2 can be represented by the following equation:

$$q^2 = \langle q^2(x, y) \rangle = \left\langle 3 \times \frac{u_{1,rms}(x, y)^2 + u_{2,rms}(x, y)^2}{2} \right\rangle. \tag{5}$$

The Taylor microscale and the corresponding Reynolds number of the flow field are, respectively, defined as follows:

$$\lambda \cong \left(\frac{5\nu q^2}{\varepsilon} \right)^{1/2}, \tag{6}$$

$$Re_\lambda \cong \frac{\lambda(q^2/3)^{1/2}}{\nu}. \tag{7}$$

The polydisperse droplets are produced by an air-assist atomizer placed about 1.1 m above the center of the HIT domain, as shown in Fig. 1(a). Figure 1(b) shows the sketch of the experimental setup. The droplet sizes and volume fractions are controlled by adjusting the inlet water flow rate and air pressure supply at the atomizer. More information concerning the atomizer can be found in Ref. 42. The droplet velocity was calculated using an in-house-developed hybrid particle tracking/particle image velocimetry algorithm. The configuration is identical to that of the PIV system, although the velocity fields of the discrete phase (droplets) and continuous phase (turbulence) are

TABLE II. Measurement of the turbulent statistics.

ν (m ² /s)	q^2 (m ² /s ²)	$u_{1,rms}/u_{2,rms}$	ε (m ² /s ³)	η (mm)	τ_η (ms)	u_η (m/s)	Re_λ
1.57×10^{-5}	0.85	1.03	1.48	0.226	3.3	0.068	227
1.57×10^{-5}	1.15	1.03	2.02	0.209	2.8	0.075	264

measured separately in this experiment, because the droplets cannot be distinguished from the tracers in the particle images by their brightness or pixel sizes. Therefore, when measuring the droplet motions in two-phase turbulence, the woofers are turned on while the tracer particles are not released in the laboratory. Nevertheless, for all two-phase flows in this experiment, the particle volume fraction Φ_V is approximately 5×10^{-6} , close to the one-way coupled regime.⁴³ This indicates that the droplet motions have little influence on the turbulent flow. The droplets are varied by adjusting the air pressure supply in the atomizer while keeping the water flow rate unchanged. The size distribution of droplets in the measurement domain is measured by a laser particle size analyzer. There are many statistical parameters for quantifying the droplet size—the arithmetic mean diameter D_{10} and the Sauter mean diameter D_{32} (Ref. 44) are commonly used. In different cases, the droplet size ranges as $d = 10\text{--}120 \mu\text{m}$ and the Sauter mean diameter D_{32} of the droplets changes slightly from 35 to 40 μm , where d is the arithmetic mean diameter. $m_{air,1}$ and $m_{air,2}$ represent two air flow rates in Fig. 2. As shown in Fig. 2(a), the droplet size is distributed in the polydisperse state. From the particle size distributions of the two cases, the mean particle diameter and mean Stokes number St can be calculated. From Fig. 2(b), St can be calculated from the distribution of the Stokes number and is 1.2916 and 1.6478 in the two cases.

III. RESULTS AND DISCUSSION

As pointed out by Wang and Maxey,⁶ the relative velocity statistics are affected by inertia in complex and profound ways. Thus, to elucidate the coupled physics, parametric evaluations are first reported to provide an idea of the influence of St and Re on the particle relative velocity, followed by detailed investigations of the second-order structure function of the particle relative velocity statistics. The particles are then categorized into clusters, voids, and intermediate cluster-void regions based on the Voronoi tessellation proposed by Monchaux.⁴⁵ The conditional second-order structure functions of the categorized particle relative velocity statistics are derived, showing for the first time that the second-order relative velocity structures of particles in clusters are low in kinetic energy and different from those of the arithmetically averaged particle statistics in both the dissipation range and the inertial subrange.

The influence of St and Re on the radial relative velocity is first evaluated for two turbulent Reynolds number and a total of four

experimental conditions. For any two particles in the particle field, such as A and B, the radial relative velocity is defined as $w_r = (v_A - v_B) \cdot (r)$, where v_i is the velocity vector of particle i , and $r = x_A - x_B$, where x_i is the position vector of particle i . The probability density function (PDF) of the radial relative velocity w_r under the two Reynolds numbers and two arithmetically averaged Stokes numbers is plotted in Fig. 3(a). From Fig. 3(a), we see that, for the same Reynolds number, the radial relative velocities of different Stokes numbers are almost the same. Thus, it can be inferred that the Stokes number does not significantly affect the radial relative velocity. Figure 3(a) also indicates that the radial relative velocity of $Re_\lambda = 264$ is larger than that of $Re_\lambda = 227$, especially at larger scales. In contrast to the effect of the Stokes number, an increase in the Reynolds number enhances the radial relative velocity of the particles, this indicates that particle dispersion is mainly governed by the carrier phase turbulence. Thus, the large-scale energy-containing fluid structures in the inertia range have a more pronounced impact on the radial relative velocity distribution, while the carrier phase has a smaller impact on the radial relative velocity probability distribution in the dissipation range.

To further quantify the impact of the Reynolds number in both the dissipation range and the inertial subrange, the difference in the velocity structure function normalized by the square of the Kolmogorov scaled velocity, defined as $S = [G_2(Re_\lambda = 264) - G_2(Re_\lambda = 227)]/u_\eta^2$, is plotted for the two Reynolds numbers in Fig. 3(b). Figure 3(b) is used to quantify the scale effect on the radial velocity distribution together with Fig. 3(a). The value of S approaches zero in the dissipation range and increases significantly in the inertial subrange, which provides additional supportive evidence that the particle radial relative velocity is largely governed by the carrier turbulent Reynolds number in the inertial subrange, but is barely affected in the dissipation range.

With the basic parametric dependence summarized above, the scaling of the second-order relative velocity structure function is now investigated in both the dissipation range and the inertial subrange. The second-order relative velocity structure function is defined as

$$G_2(r, St) = \langle [\Delta v]^2 \rangle, \tag{8}$$

where $\Delta v(r, St) = v(x + r, St) - v(x, St)$, $v(r, St)$ is the particle velocity at the x coordinate, $St = \tau_p/\tau_\eta$ is the Stokes number of the particle (which is a dimensionless measure of particle inertia), $\tau_p =$

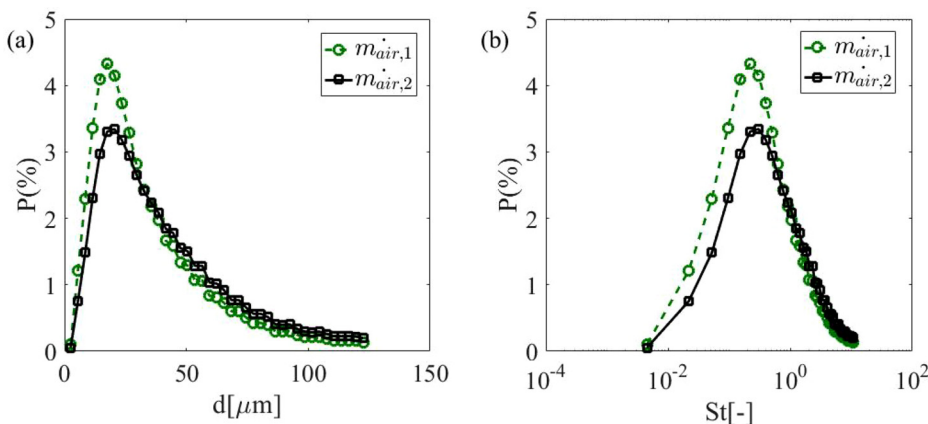


FIG. 2. (a) Physical size distributions of droplets measured by laser particle size analyzer in the measurement domain for two air flow rates in the atomizer. (b) Distribution of droplet Stokes number for two air flow rates in the atomizer.

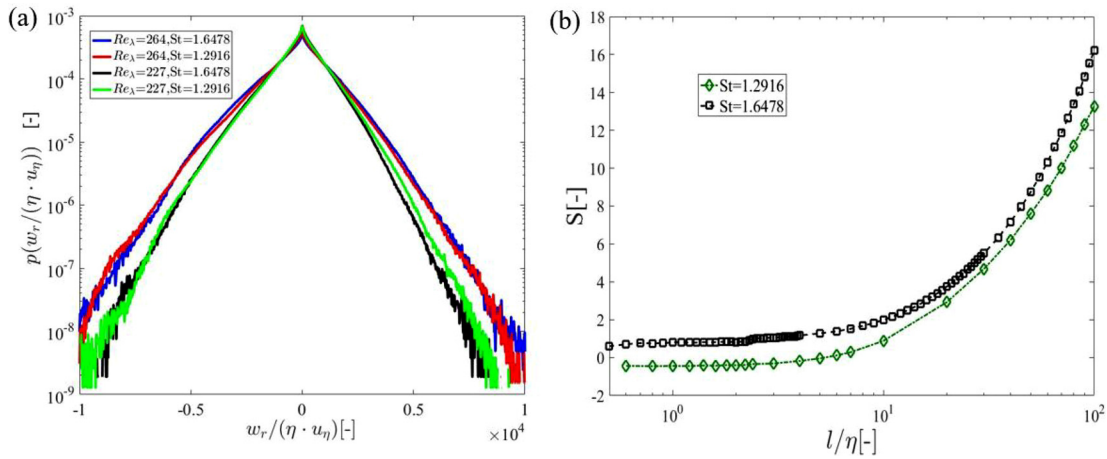


FIG. 3. (a) Probability density functions of the radial relative velocity for two turbulent Reynolds number and a total of four experimental conditions. (b) Difference of velocity structure function normalized by the square of the Kolmogorov velocity of two Reynolds numbers, $S = [G_2(Re_\lambda = 264) - G_2(Re_\lambda = 227)]/u_\eta^2$.

$(\rho_p d^2)/18\rho\nu$ is the particle relaxation time, $\tau_\eta = \sqrt{\nu/\langle \epsilon \rangle}$ is the Kolmogorov timescale, d is the particle diameter, ρ_p is the particle density, ρ is the density of the carrier phase fluid, ν is the kinematic viscosity of the carrier phase fluid, and ϵ is the turbulent kinetic energy dissipation rate. Kolmogorov proposed three hypotheses that constitute the classic K41 theory. The hypothesis of local isotropy states that the small-scale turbulence is isotropic when Re_λ is sufficiently large and the flow field is far from the boundaries. Based on the K41 theory, the second-order structure function $G_2(r, St = 0)$ is defined as

$$G_2(r, St = 0) = \begin{cases} C_2[\langle \epsilon \rangle r]^{\frac{2}{3}}, & \eta \ll r \ll l_{EI}, \\ \frac{\langle \epsilon \rangle}{15\nu} r^2, & r \ll \eta. \end{cases} \quad (9)$$

As indicated from the above equation, the second-order velocity structure function of the fluid particles follows the scaling r^2 in the dissipation range. The stationary homogeneous and isotropic turbulence generated in this experiment falls well within the Kolmogorov assumptions. The second-order velocity structure functions of the particles are evaluated and plotted in Fig. 4 for the two turbulent Reynolds

numbers and four experimental conditions. In Fig. 4, U represents the velocity component in the horizontal direction x_1 and V represents the velocity component in the gravity direction x_2 , $S^2 = G_2/u_\eta^2$.

Figure 4 shows that, in the dissipation range, there is an obvious departure between the second-order structure function of particles normalized by the square of the Kolmogorov velocity for all four experimental conditions and the Kolmogorov turbulent scaling of r^2 . In the inertial range, the second-order structure function normalized by the square of the Kolmogorov velocity is consistent with the scale form of $r^{2/3}$. The Stokes numbers are relatively close in the four experimental conditions and so the slopes in the dissipation range are quite similar for the different Stokes numbers. The experiment in which $Re_\lambda = 227$ and $St = 1.2916$ gives slightly different results in the dissipation range than the other three conditions.

These observations can be explained by the caustic or sling effect, which indicates that relative velocity differences Δv may not reduce to zero smoothly as the particle separation decreases in the presence of inertia. This is possibly due to the dissipative particle dynamics in the phase space and the folding of the ensemble of particle trajectories evolving in the velocity direction. The effect of caustics becomes

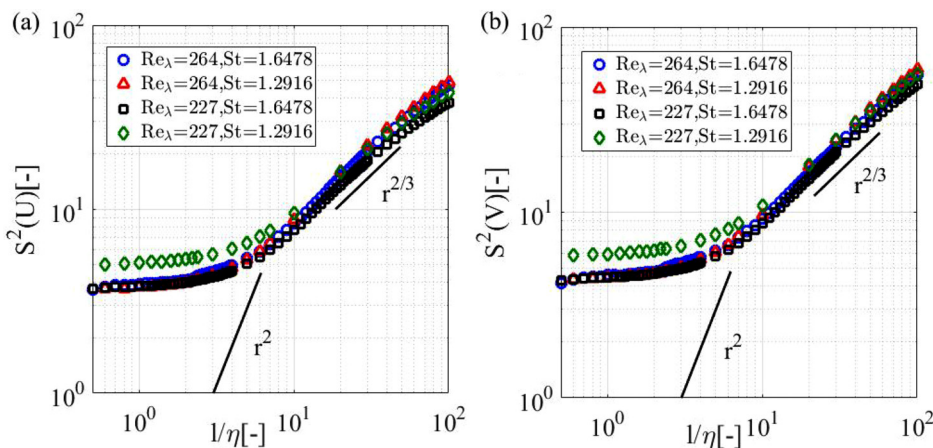


FIG. 4. (a) Second-order structure function normalized by the square of the Kolmogorov velocity of the horizontal velocity U for four experimental conditions. (b) Second-order structure function normalized by the square of the Kolmogorov velocity of the vertical velocity V for four experimental conditions.

significant when inertia dominates and the particle response time is greater than the turbulent flow timescale. In this case, adjacent particles are more likely to have uncorrelated velocities and, as a consequence, form dense caustics in space and time. Bec *et al.*⁴ proposed the following scaling form for the dispersed particles:

$$G_p(r, St) \propto r^{\xi_p(St)}, \tag{10}$$

where $0 \leq \xi_p(St) \leq p$. This assumption is consistent with the limits $\xi_p(St \rightarrow 0) = p$ and $\xi_p(St \rightarrow \infty) = 0$. For intermediate values of the Stokes number, Bec *et al.*⁴ performed a sweep of the Stokes number based on direct numerical simulations. The fitted results yielded the following expression:

$$\xi_p(St) = \begin{cases} p, & p \leq \alpha \ln(7/St), \\ \alpha \ln(7/St), & St \leq 7, \\ 0, & St > 7. \end{cases} \tag{11}$$

To evaluate these empirical scaling forms based on direct numerical simulations, the fitting slopes ξ of the four experimental conditions in the dissipation range are presented in Table III. From Table III, the scaling in the dissipation range of $St = 1.2916$ is equal to that of $St = 1.6478$ for $Re_\lambda = 264$. The scaling form proposed by Bec *et al.*⁴ is $\alpha \ln(7/St)$ in this case. As indicated in Fig. 4, caustics form in the dissipation range, consistent with previous studies, yet two contradictions occur. First, the negative correlation with the Stokes number is not observed perhaps because the St numbers used are too close. Second, the value of α is considered to be a linear metric that is independent of the Reynolds number, but a slight difference is observed between $Re_\lambda = 227$ and $Re_\lambda = 264$, which indicates that although inertia governs the dissipation range, the particle dynamics are still affected by the carrier phase turbulence. These two contradictions are possibly due to polydispersity and the particle dynamics may be affected by the carrier-phase-governed preferential concentration; thus, St , which is the arithmetic average between the particle and fluid time scales, does not represent the overall particle dynamics. Hence, it is desirable to gain a basic understanding of the second-order structure function of particle relative velocity statistics in the cluster and void regions.

Thus far, parametric evaluations have been reported to provide an idea of how the Stokes number and Reynolds number influence the particle relative velocity, followed by an investigation of the second-order structure function of the particle relative velocity statistics. The large-scale energy-containing fluid structures at the inertia range have a more pronounced impact on the radial relative velocity distribution, while in the dissipation range, the carrier phase has a smaller impact on the radial relative velocity probability distribution. Additionally, in the dissipation range, there is an obvious departure between the second-order structure function of particles normalized by the square of the Kolmogorov velocity and the Kolmogorov turbulent scaling of r^2 for all four experimental conditions. In the inertial range, the second-order structure function normalized by the square of the

TABLE III. Fitting slopes of four experimental cases in dissipation range.

	$St = 1.2916$	$St = 1.6478$
$Re_\lambda = 264$	0.06	0.06
$Re_\lambda = 227$	0.05	0.05

Kolmogorov velocity is consistent with the scale form of $r^{2/3}$. The scaling form in the dissipation range is not only governed by inertia, but also by the carrier phase turbulence and possibly by preferential concentration. However, the second-order structure functions of the particle relative velocity statistics in the cluster and void regions have not previously been reported. In this paper, the particles are categorized into clusters, voids, and intermediate cluster-void regions based on the Voronoi tessellation proposed by Monchaux *et al.*⁴⁵ The conditional second-order structure functions of the categorized particle relative velocity statistics are now derived and reported for the first time. Particles dispersed in the flow field can be divided into different types using a Voronoi diagram, which is a method for obtaining the particle concentration field. As shown in Fig. 5(a), the spatial domain of a set of discrete particles is uniquely divided into a series of nonoverlapped Voronoi cells, each of which is occupied by one individual particle. In this paper, we use the normalized Voronoi area,⁴⁶ given by

$$\gamma(x, y, t) = A(x, y, t)/\bar{A}(x, y), \tag{12}$$

where $\bar{A}(x, y)$ is the time-averaged area of the Voronoi cell area at (x, y) , which is used to eliminate the inhomogeneity of the spatial distribution of particles. The inverse of γ can be used as a measure of the local particle concentration associated with the turbulent effect. Following Monchaux *et al.*,⁴⁵ the profiles of PDF(γ) are compared with that of the random Poisson process to determine the clustering feature of discrete particles in turbulent flows. As shown in Fig. 5(b), there are two intersections between these two curves. When γ is less than γ_C , these particles are regarded as cluster particles. When γ is greater than γ_V , these particles are regarded as void particles. Particles are regarded as cluster-void particles when γ is between γ_C and γ_V . For the four cases presented here, the intersections are $\gamma_C \approx 0.65$ and $\gamma_V \approx 2.1$, both of which are quasi-independent of Re_λ and St . According to the above-mentioned methods, particles are divided into clusters, cluster-voids, and voids, and the characteristics of these three types are compared as follows.

In Figs. 6 and 7, U represents the velocity component in the horizontal direction x_1 and V represents the velocity component in the gravity direction x_2 . The second-order velocity structure function of cluster, cluster-void, void, and all particles of U are calculated in the four experimental conditions. As shown in Fig. 6, the conditional second-order structure functions of the categorized particle relative velocity U have been derived for the first time. The conditional second-order relative velocity structure function of particles in clusters is low in kinetic energy and differs from that of the arithmetically averaged particle statistics in both the dissipation range and the inertial subrange. In the dissipation range, the caustics are present for all categories of particles. The scaling forms of the second-order velocity structure functions of these types of particles are different in the dissipation range, with the cluster particles having the lowest slope and void particles having the steepest slope. In the inertial range, the scaling of the second-order velocity structure functions is almost identical for all categories of particles. From the dissipation range to the inertial subrange, a transition region occurs in which the scaling form of the second-order velocity structure functions of the void particles, cluster-void particles, and cluster particles is similar, suggesting a multifractal nature. Figure 7 presents the second-order velocity structure functions of V for the clustered, intermediate, voided, and arithmetically averaged particles. The results exhibit the same trends as in the horizontal

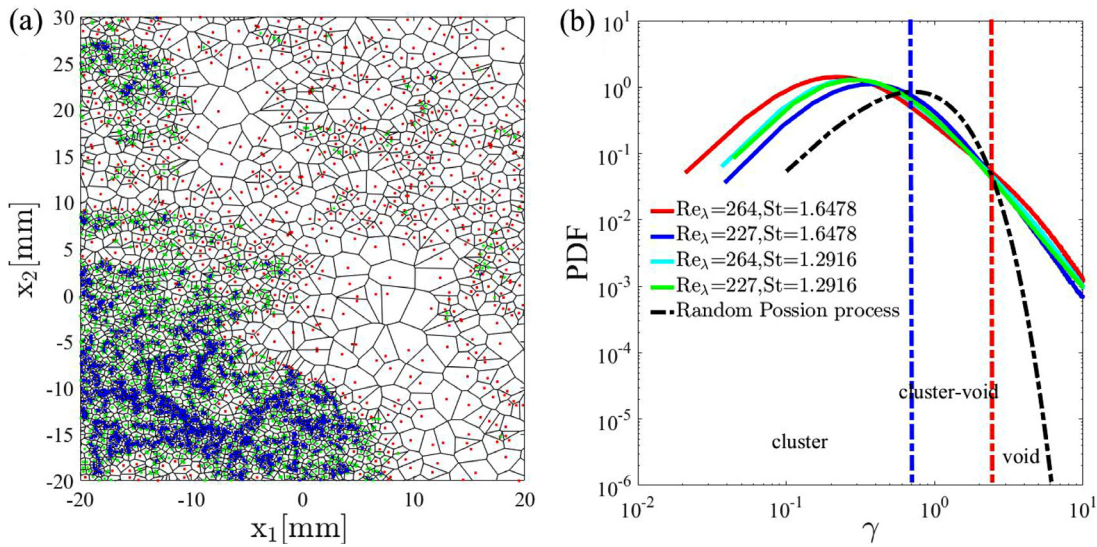


FIG. 5. (a) Voronoi diagrams of the spatial distribution of particles as denoted by blue dots, green dots, and red dots. (b) PDFs of dimensionless Voronoi cell area γ for different cases. The PDF for a random Poisson process is shown as a black dashed-dotted line, whose two intersections with the γ -PDF profiles yield the thresholds $\gamma_C = 0.65$ and $\gamma_V = 2.1$ for clusters and voids, respectively.

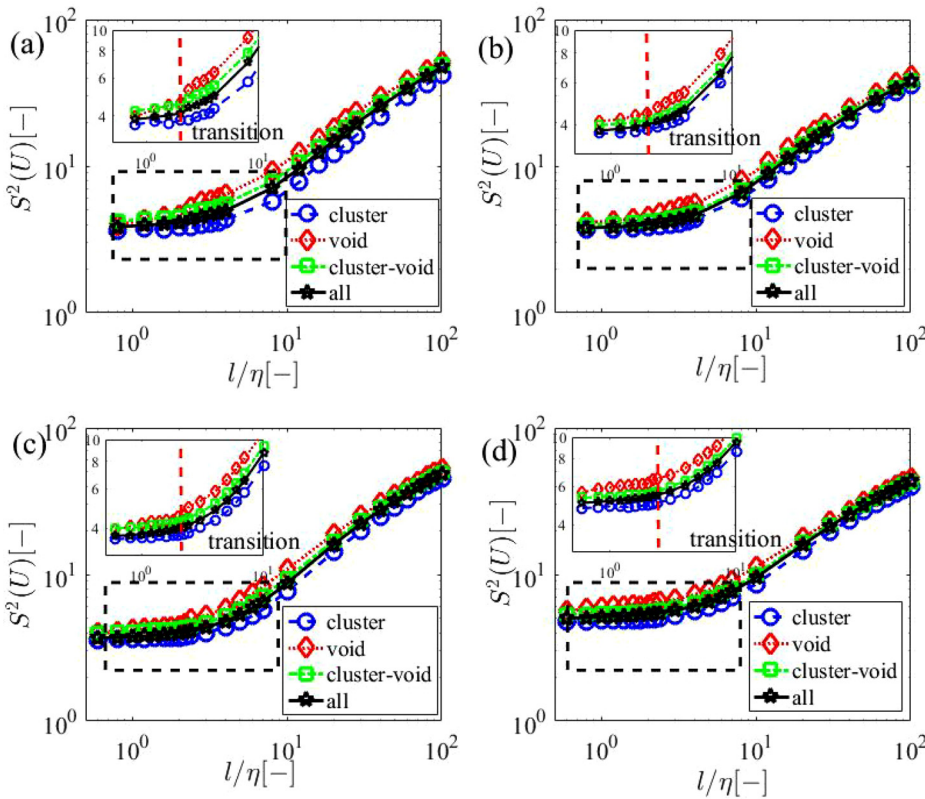


FIG. 6. Velocity structure function of cluster particles, cluster-void particles, void particles, and all particles of U . (a) $Re_\lambda = 264$, $St = 1.6478$; (b) $Re_\lambda = 227$, $St = 1.6478$; (c) $Re_\lambda = 264$, $St = 1.2916$; and (d) $Re_\lambda = 227$, $St = 1.2916$.

direction in both the dissipation and the inertial range. Some differences are observed in the absolute intensity of the second-order velocity structure functions of U and V . In addition, the difference in the second-order velocity structure functions between the void particles

and cluster-void particles is smaller for V than for U , possibly due to the presence of gravity.

As shown in Fig. 8, the ratio of the second-order velocity structure functions of V and U is greater than one for all types of particles,

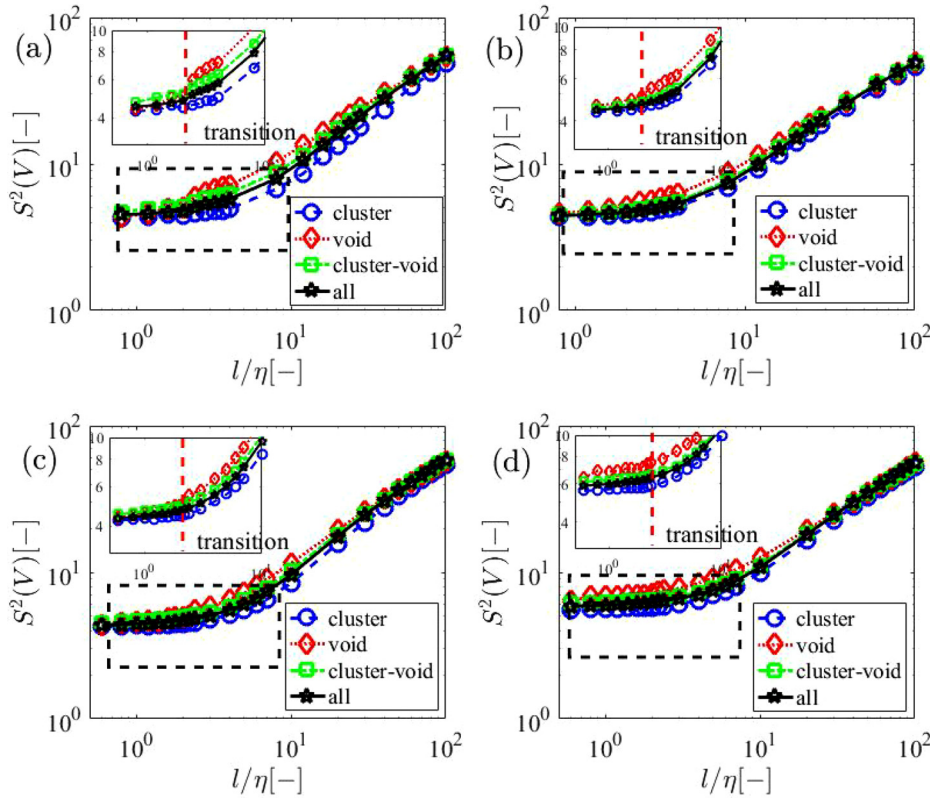


FIG. 7. Velocity structure function of cluster particles, cluster-void particles, void particles, and all particles of V . (a) $Re_\lambda = 264$, $St = 1.6478$; (b) $Re_\lambda = 227$, $St = 1.6478$; (c) $Re_\lambda = 264$, $St = 1.2916$; and (d) $Re_\lambda = 227$, $St = 1.2916$.

indicating that the influence of gravity is significant in all experimental conditions. The ratio first decreases and then increases from the dissipation range to the inertial range, with a minimum value at about $l/\eta = 20$. Thus, the effect of gravity is related to this scale, and in the inertial range, the influence of gravity is more pronounced at larger scales. The ratio of the second-order velocity structure functions of V and U for voided particles is obviously lower than for other particle types, suggesting that voided particles are less affected by gravity than clustered particles.

To further elucidate the different mechanism for the clustered and voided particles, Fig. 9 illustrates k_p among the clustered, intermediate, and voided particles, in which $k_p = \frac{1}{2} \langle v^2 \rangle$ is the average particle kinetic energy per unit mass. The voided particles are high in kinetic energy, and the clustered particles are low in kinetic energy. For the energy-containing scales, the second-order structure function follows the scale form of $r^{2/3}$, suggesting that the particle kinetic energy is governed by the carrier phase kinetic energy and the particle dispersion is influenced by the energy-containing flow structures. This is evidence that clustered particles with high concentrations are most likely to be spatially correlated with low-kinetic-energy flow structures and the voided particles are more likely to be related to high-kinetic-energy flow structures.

IV. CONCLUSION

To provide experimental evidence for the formation of caustics and their possible coupling effects on preferential clustering, this paper

has reported high-resolution particle velocity measurements under four experimental conditions and evaluated the particle relative velocity probability function and second-order relative velocity structure function from the dissipation range to the inertial subrange. The particles were categorized into clusters, voids, and intermediate cluster-void regions based on Voronoi tessellation, and the conditional second-order structure functions of the categorized particle relative velocity statistics were derived and reported for the first time. The conclusions can be summarized as follows:

- (1) Parametric evaluations were first reported to provide an idea of how the Stokes number and Reynolds number influence the particle relative velocity probability function. The large-scale energy-containing fluid structures in the inertia range have a more pronounced impact on the radial relative velocity distribution, while in the dissipation range, the carrier phase has a smaller impact on the radial relative velocity probability distribution.
- (2) The second-order relative velocity structure function of particles was investigated. In the dissipation range, an obvious departure between the second-order structure function of particles normalized by the square of the Kolmogorov velocity and the Kolmogorov turbulent scaling of r^2 was observed for all four experimental conditions. In the inertial range, the second-order structure function normalized by the square of the Kolmogorov velocity was consistent with the scale form of $r^{2/3}$ in all cases.

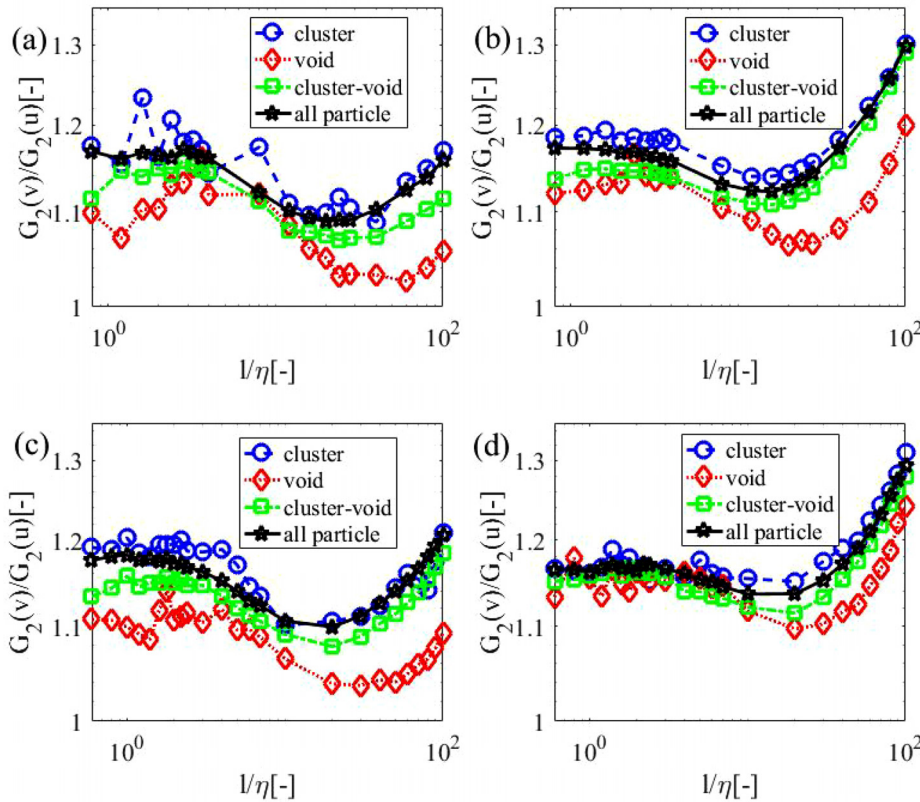


FIG. 8. Ratio of velocity structure functions of V and U for cluster particles, cluster-void particles, void particles, and all particles. (a) $Re_\lambda = 264$, $St = 1.6478$; (b) $Re_\lambda = 227$, $St = 1.6478$; (c) $Re_\lambda = 264$, $St = 1.2916$; and (d) $Re_\lambda = 227$, $St = 1.2916$.

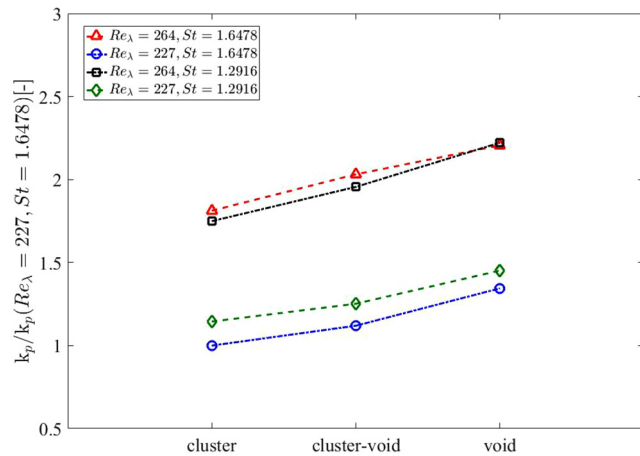


FIG. 9. Average particle kinetic energy per unit mass of cluster particles, cluster-void particles, and void particles in the four experimental cases.

(3) The conditional second-order relative velocity structure function of particles in clusters differs from that of the arithmetically averaged particle statistics in both the dissipation range and the inertial subrange. In the dissipation range, caustics are present for all categories of particles. In the inertial range, the scaling of the second-order velocity structure function is almost identical for all categorized particle types. From the dissipation

range to the inertial subrange, a transition region appears in which the scaling form of the second-order velocity structure functions of the void particles, cluster-void particles, and cluster particles is similar, suggesting a multifractal nature.

(4) The categorized particles are mostly likely governed by different flow structures and respond differently to gravity. The voided particles contain higher kinetic energy and the clustered particles are low in kinetic energy. This is evidence that clustered particles with high concentrations are most likely spatially correlated to the low-kinetic-energy flow structures and the voided particles are more likely to be related to high-kinetic-energy flow structures. The ratio of the second-order velocity structure functions of V and U for voided particles is obviously lower than for other particle types, suggesting that voided particles are less affected by gravity than clustered particles.

ACKNOWLEDGMENTS

Tuo Li greatly appreciates the assistance of Hang-Yu Zhu in the experiments. We wish to acknowledge financial support from the National Natural Science Foundation of China (Grant Nos. 91941104 and 11872366).

AUTHOR DECLARATIONS

Conflict of Interest

The authors have no conflicts to disclose.

Author Contributions

Tuo Li: Conceptualization (equal); Data curation (equal); Formal analysis (equal); Investigation (equal); Methodology (equal); Project administration (equal); Software (equal); Writing – original draft (equal). **Xinyang Li:** Investigation (equal); Methodology (equal); Software (equal). **Huan Lian:** Funding acquisition (equal); Investigation (equal); Methodology (equal); Project administration (equal); Resources (equal); Writing – review & editing (equal).

DATA AVAILABILITY

The data that support the findings of this study are available from the corresponding author upon reasonable request.

NOMENCLATURE

$\bar{A}(x, y)$	the time-averaged area of the Voronoi cell area
d	the particle diameter
$G_2(r, St) = \langle [\Delta v]^2 \rangle$	the second-order relative velocity structure function
$k_p = \frac{1}{2} \langle v^2 \rangle$	the average particle kinetic energy per unit mass
q^2	the ensemble-averaged turbulent kinetic energy
Re_λ	the Taylor microscale Reynolds number of the flow field
$S = [G_2(Re_\lambda = 264) - G_2(Re_\lambda = 227)]/u_\eta^2$	difference of velocity structure function normalized by the square of the Kolmogorov velocity of two Reynolds numbers
$S^2 = G_2/u_\eta^2$	the second-order relative velocity structure function normalized by the square of the Kolmogorov velocity
u_η	the Kolmogorov velocity scale
v	the particle velocity
$\gamma(x, y, t) = A(x, y, t)/\bar{A}(x, y)$	the normalized Voronoi area
ε	the turbulent kinetic energy dissipation rate
η	the Kolmogorov length scale
λ	the Taylor microscale
ν	the kinematic viscosity of the carrier phase fluid
ρ	the density of the carrier phase fluid
ρ_p	THE particle density
$\tau_p = (\rho_p d^2)/18\rho\nu$	the particle relaxation time
τ_η	the timescale of the minimum vortex structure
$\tau_\eta = \sqrt{\nu/\langle \varepsilon \rangle}$	the Kolmogorov timescale

REFERENCES

- Sundaram and L. R. Collins, "Collision statistics in an isotropic particle-laden turbulent suspension. Part 1. Direct numerical simulations," *J. Fluid Mech.* **335**, 75–109 (1997).
- D. A. McQuarrie, *Statistical Mechanics* (Harper & Row Publishers, 1976).
- M. R. Maxey, "The gravitational settling of aerosol particles in homogeneous turbulence and random flow fields," *J. Fluid Mech.* **174**, 441–465 (1987).
- J. Bec, L. Biferale, M. Cencini, A. S. Lanotte, and F. Toschi, "Intermittency in the velocity distribution of heavy particles in turbulence," *J. Fluid Mech.* **646**, 527–536 (2010).
- K. D. Squires and J. K. Eaton, "Preferential concentration of particles by turbulence," *Phys. Fluids A* **3**, 1169–1178 (1991).
- L.-P. Wang and M. R. Maxey, "Settling velocity and concentration distribution of heavy particles in homogeneous isotropic turbulence," *J. Fluid Mech.* **256**, 27–68 (1993).
- R. A. Shaw, W. C. Reade, L. R. Collins, and J. Verlinde, "Preferential concentration of cloud droplets by turbulence: Effects on the early evolution of cumulus cloud droplet spectra," *J. Atmos. Sci.* **55**, 1965–1976 (1998).
- W. C. Reade and L. R. Collins, "Effect of preferential concentration on turbulent collision rates," *Phys. Fluids* **12**, 2530–2540 (2000).
- L. R. Collins and A. Keswani, "Reynolds number scaling of particle clustering in turbulent aerosols," *New J. Phys.* **6**, 119 (2004).
- J. K. Eaton and J. R. Fessler, "Preferential concentration of particles by turbulence," *Int. J. Multiphase Flow* **20**, 169–209 (1994).
- A. M. Wood, W. Hwang, and J. K. Eaton, "Preferential concentration of particles in homogeneous and isotropic turbulence," *Int. J. Multiphase Flow* **31**, 1220–1230 (2005).
- J. P. Salazar, J. De Jong, L. Cao, S. H. Woodward, H. Meng, and L. R. Collins, "Experimental and numerical investigation of inertial particle clustering in isotropic turbulence," *J. Fluid Mech.* **600**, 245–256 (2008).
- E. W. Saw, R. A. Shaw, S. Ayyalasomayajula, P. Y. Chuang, and A. Gylfason, "Inertial clustering of particles in high-Reynolds-number turbulence," *Phys. Rev. Lett.* **100**, 214501 (2008).
- J. De Jong, J. P. Salazar, S. H. Woodward, L. R. Collins, and H. Meng, "Measurement of inertial particle clustering and relative velocity statistics in isotropic turbulence using holographic imaging," *Int. J. Multiphase Flow* **36**, 324–332 (2010).
- L.-P. Wang, A. S. Wexler, and Y. Zhou, "Statistical mechanical description and modelling of turbulent collision of inertial particles," *J. Fluid Mech.* **415**, 117–153 (2000).
- Y. Zhou, A. S. Wexler, and L.-P. Wang, "Modelling turbulent collision of bidisperse inertial particles," *J. Fluid Mech.* **433**, 77–104 (2001).
- L. I. Zaichik and V. M. Alipchenkov, "Pair dispersion and preferential concentration of particles in isotropic turbulence," *Phys. Fluids* **15**, 1776–1787 (2003).
- J. Chun, D. L. Koch, S. L. Rani, A. Ahluwalia, and L. R. Collins, "Clustering of aerosol particles in isotropic turbulence," *J. Fluid Mech.* **536**, 219–251 (2005).
- O. Ayala, B. Rosa, L.-P. Wang, and W. W. Grabowski, "Effects of turbulence on the geometric collision rate of sedimenting droplets. Part 1. Results from direct numerical simulation," *New J. Phys.* **10**, 075015 (2008).
- S. Goto and J. Vassilicos, "Sweep-stick mechanism of heavy particle clustering in fluid turbulence," *Phys. Rev. Lett.* **100**, 054503 (2008).
- S. W. Coleman and J. C. Vassilicos, "A unified sweep-stick mechanism to explain particle clustering in two- and three-dimensional homogeneous, isotropic turbulence," *Phys. Fluids* **21**, 113301 (2009).
- L. I. Zaichik and V. M. Alipchenkov, "Statistical models for predicting pair dispersion and particle clustering in isotropic turbulence and their applications," *New J. Phys.* **11**, 103018 (2009).
- L. Chen, S. Goto, and J. C. Vassilicos, "Turbulent clustering of stagnation points and inertial particles," *J. Fluid Mech.* **553**, 143–154 (2006).
- J. Bec, L. Biferale, M. Cencini, A. Lanotte, S. Musacchio, and F. Toschi, "Heavy particle concentration in turbulence at dissipative and inertial scales," *Phys. Rev. Lett.* **98**, 084502 (2007).
- S. Balachandar and J. K. Eaton, "Turbulent dispersed multiphase flow," *Annu. Rev. Fluid Mech.* **42**, 111–133 (2010).
- J. Tom and A. D. Bragg, "Multiscale preferential sweeping of particles settling in turbulence," *J. Fluid Mech.* **871**, 244–270 (2019).
- G. Falkovich, A. Fouxon, and M. G. Stepanov, "Acceleration of rain initiation by cloud turbulence," *Nature* **419**, 151–154 (2002).
- G. Falkovich and A. Pumir, "Sling effect in collisions of water droplets in turbulent clouds," *J. Atmos. Sci.* **64**, 4497–4505 (2007).

- ²⁹M. Wilkinson, B. Mehlig, and V. Bezuglyy, “Caustic activation of rain showers,” *Phys. Rev. Lett.* **97**, 048501 (2006).
- ³⁰L. Ducas and A. Pumir, “Inertial particle collisions in turbulent synthetic flows: Quantifying the sling effect,” *Phys. Rev. E* **80**, 066312 (2009).
- ³¹M. I. Yudine, “Physical considerations on heavy-particle diffusion,” *Adv. Geophys.* **6**, 185–191 (1959).
- ³²G. P. Bewley, E.-W. Saw, and E. Bodenschatz, “Observation of the sling effect,” *New J. Phys.* **15**, 083051 (2013).
- ³³Z. Dou, P. J. Ireland, A. D. Bragg, Z. Liang, L. R. Collins, and H. Meng, “Particle-pair relative velocity measurement in high-Reynolds-number homogeneous and isotropic turbulence using 4-frame particle tracking velocimetry,” *Exp. Fluids* **59**, 30 (2018).
- ³⁴M. A. Yavuz, R. P. J. Kunnen, G. J. F. Van Heijst, and H. J. H. Clercx, “Extreme small-scale clustering of droplets in turbulence driven by hydrodynamic interactions,” *Phys. Rev. Lett.* **120**, 244504 (2018).
- ³⁵M. R. Maxey and J. J. Riley, “Equation of motion for a small rigid sphere in a nonuniform flow,” *Phys. Fluids* **26**, 883–889 (1983).
- ³⁶R. Gatignol, “The Faxén formulae for a rigid particle in an unsteady non-uniform Stokes flow,” *J. Mec. Theor. Appl.* **1**, 143–160 (1983).
- ³⁷L. Brandt and F. Coletti, “Particle-laden turbulence: Progress and perspectives,” *Annu. Rev. Fluid Mech.* **54**, 159–189 (2022).
- ³⁸H. Zhu, C. Pan, and H. Lian, “Spatial correlations and relative velocities of polydisperse droplets in homogeneous isotropic turbulence,” *Phys. Fluids* **34**, 083320 (2022).
- ³⁹F. Scarano and M. L. Riethmuller, “Advances in iterative multigrid PIV image processing,” *Exp. Fluids* **29**, S051–S060 (2000).
- ⁴⁰O. R. H. Buxton, S. Laizet, and B. Ganapathisubramani, “The effects of resolution and noise on kinematic features of fine-scale turbulence,” *Exp. Fluids* **51**, 1417–1437 (2011).
- ⁴¹U. Frisch, *Turbulence: The Legacy of A.N. Kolmogorov* (Cambridge University Press, 1995).
- ⁴²H. Lian, G. Charalampous, and Y. Hardalupas, “Preferential concentration of poly-dispersed droplets in stationary isotropic turbulence,” *Exp. Fluids* **54**, 1525 (2013).
- ⁴³S. Elghobashi, “On predicting particle-laden turbulent flows,” *Appl. Sci. Res.* **52**, 309–329 (1994).
- ⁴⁴N. Pandurangan and S. Sahu, “Spatial evolution of multi-scale droplet clusters in an evaporating spray,” *Phys. Fluids* **34**, 113310 (2022).
- ⁴⁵R. Monchaux, M. Bourgoin, and A. Cartellier, “Preferential concentration of heavy particles: A Voronoï analysis,” *Phys. Fluids* **22**, 103304 (2010).
- ⁴⁶A. J. Petersen, L. Baker, and F. Coletti, “Experimental study of inertial particles clustering and settling in homogeneous turbulence,” *J. Fluid Mech.* **864**, 925–970 (2019).